Preparation and Catalytic Evaluation of Macroporous Crystalline Sulfated Zirconium Dioxide Templated with Colloidal Crystals

Mohammed A. Al-Daous and Andreas Stein*

Department of Chemistry, University of Minnesota, Minneapolis, Minnesota 55455

Received January 8, 2003. Revised Manuscript Received April 21, 2003

Colloidal crystal templates were used to synthesize three-dimensionally ordered macroporous sulfated zirconia catalysts with pore diameters of ∼300 nm and less. Ordered arrays of uniformly sized poly(methyl methacrylate) latex spheres were infiltrated with clear precursor solutions containing varying SO_4/Zr molar ratios. After solidification of the material in the void space between the spheres, the polymer templates were removed by calcination at various temperatures, producing crystalline sulfated zirconia replicas of the template arrays. The effects of changing sulfate content and calcination temperature on the physicochemical properties of the material (including shrinkage, grain size, surface area, and composition) were systematically studied. The presence of sulfate retarded the crystallization and crystal growth, which enabled greater control of macropore shrinkage and periodic order of the material. The combination of crystal growth inhibition and the inherent porosity of the PMMA latex are believed to be the major factors contributing to the observed BET surface areas of the materials, which were significantly larger than those of their nontemplated counterparts and passed through a maximum as a function of calcination temperature and initial SO_4/Zr ratio. The maximum value of 123 m^2/g was attained by a sample with SO_4/Zr = 2, calcined at 650 °C, with a sulfate surface coverage of 3.1 nm^{-2}. The *n*-butane isomerization activity of the material also passed through a maximum as a function of calcination temperature and initial SO_4/Zr ratio, reaching its maximum value for a sample with SO_4/Zr = 2, calcined at 600 °C.

Introduction

With ongoing demands for cleaner fuel, there is a growing move to eliminate aromatics and olefins from gasoline and use branched alkanes and other compounds instead to maintain high octane ratings.[1] Sulfated zirconia is an attractive, strongly acidic catalyst for isomerizing straight-chain alkanes because the solid is active at low temperatures, which favor isomerization over cracking of alkanes.[1−4] Conventional preparations of this catalyst lead to microporous materials of high catalytic activity for reactions of small molecules in the vapor phase.[5] Microporous catalysts are, however, less suited for liquid-phase processes of large molecules.[6] Mesoporous sulfated zirconia can be obtained by surfactant-templated syntheses; however, the walls in these materials are only partially crystalline.[6] The incentive for the present work is, therefore, to prepare crystalline sulfated zirconia catalysts with large, periodically ordered, connected, and uniform macropores. Such a structure would have a surface area accessible to large guest molecules used in liquid-phase catalysis and sites of high catalytic activity comparable to that of conventionally prepared sulfated zirconia catalysts. This catalyst has the potential to benefit not only the isomerization process of long-chain alkanes, but also to be used to reduce the large amounts of plastic wastes consigned to landfills,[7] where sulfated zirconia has been shown to be active in hydrocracking long-chain polyolefin materials, such as polyethylene and polypropylene, to produce either gasoline-range isoalkanes or a mixture of isobutane and isopentane.[8] In addition, these hydrogen-rich waste plastics can also be co-processed with carbon-rich coal over macroporous sulfated zirconia catalysts to produce liquid fuels or chemical feedstocks.[9]

Three-dimensionally ordered macroporous (3DOM) zirconia was initially prepared in our laboratory by using ethanol-diluted zirconium *n*-propoxide with a polystyrene colloidal crystal as the template.[10] After template removal by calcination at 575 °C for 7 h in air, the resulting zirconia had a surface area of ∼9 m^2/g, and its walls consisted of large crystallites of the

(1) Bell, A. T.; Manzer, L. E.; Chen, N. Y.; Weekman, V. W.; Hegedus, L. L.; Pereira, C. J. *Chem. Eng. Prog.* **1995**, 26−34.
(2) Song, X.; Sayari, A. *Catal. Rev.-Sci. Eng.* **1996**, *38*, 329−412.
(3) Arata, K. *Adv. Catal.* **1990**, *37*, 165−211.
(4) Gates, B. C.; Katzer, J. R.; Shuit, G. C. A. *Chemistry of Catalytic Processes*; McGraw-Hill: New York, 1979.
(5) Mercera, P. D. L.; Van Ommen, J. G.; Doesburg, E. B. M.; Burggraaf, A. J.; Ross, J. R. H. *Appl. Catal.* **1990**, *57*, 127−148.
(6) Huang, Y.-Y.; McCarthy, T. J.; Sachtler, W. M. H. *Appl. Catal. A* **1996**, *148*, 135−154.
(7) U.S. Environmental Protection Agency (EPA) Office of Solid Waste. Publication No. EPA530-R-94-042; U.S. Environmental Protection Agency, U.S. Government Printing Office: Washington, DC, 1994.
(8) Venkatesh, K. R.; Hu, J.; Wang, W.; Holder, G. D.; Tierney, J. W.; Wender, I. *Energy Fuels* **1996**, *10*, 1163−1170.
(9) Liu, K.; Meuzelaar, H. L. C. *Fuel Process. Technol.* **1996**, *49*, 1−15.
(10) Holland, B. T.; Blanford, C. F.; Do, T.; Stein, A. *Chem. Mater.* **1999**, *11*, 795−805.

10.1021/cm030019b CCC: $25.00
Published on Web 05/20/2003

monoclinic baddeleyite phase.[10] Subsequent attempts to reduce the size of the crystallites and to produce materials with the catalytically active zirconia tetragonal phase[2,3,11] involved controlling the hydrolysis of the electropositive metal alkoxide with the addition of limited amounts of sulfuric and nitric acids[12,13] in a so-called "one-step" synthesis method.[14] Using this sol to infiltrate a prepacked bed of poly(methyl methacrylate) (PMMA) colloidal crystals produced, upon calcination at 550 °C, brightly colored but catalytically inactive materials. The bright colors were due to diffraction of light from the ordered periodic structure, combined with a relatively small crystallite size within the wall skeleton.[15,16] Further attempts involved the use of zirconium acetate stabilized in dilute acetic acid[12] to prepare a homogeneous, clear precursor solution containing sulfate ions introduced by the addition of ammonium sulfate. Calcination at 600 °C produced an opalescent material with a relatively low catalytic activity in *n*-butane isomerization reactions. By using sulfuric acid and zirconyl nitrate, a clear homogeneous precursor solution could be prepared that enabled the formation of a catalyst with an appreciable catalytic activity and allowed for greater manipulation of the final structure of the material.

In the present work, this clear precursor solution was used to infiltrate a PMMA colloidal crystal template. Once the precipitate hardened, the template was removed by calcination to produce 3DOM crystalline sulfated zirconia. The materials were characterized by a range of physical methods to interpret the effects of synthesis parameters on the properties of the resulting 3DOM structure, with emphasis on the identification of factors affecting the shrinkage of the macropores, surface area, and pore wall crystallinity. The materials were tested as catalysts for the isomerization of *n*-butane to evaluate the catalytic activity of available active sites.

Experimental Section

Materials. Non-cross-linked, monodisperse poly(methyl methacrylate) latex spheres were synthesized using an emulsifier-free emulsion polymerization technique according to literature reports.[16,17] As described in the reported syntheses, variations in reaction temperature and concentrations allow for the preparation of monodisperse latex spheres with diameters ranging from ~300 to 500 nm with small standard deviations within a batch (≤4 nm). Before use, the spheres were close-packed into colloidal crystals by gravity sedimentation followed by drying at room temperature. Zirconium oxynitrate hydrate $ZrO(NO_3)_2{\cdot}xH_2O$ (technical grade, $x \approx 6$), sulfuric acid (95−98%, certified ACS), and methanol (99.08%, ACS reagent) were obtained from Aldrich. All precursors were used as received without further purification.

Synthesis of 3DOM Sulfated Zirconia. Zirconium oxynitrate was dissolved in a 1 M aqueous nitric acid solution to a concentration of ~1.7 M. Each sample was synthesized using a total of 30 mL of solution composed of sulfuric acid, zirconyl nitrate solution, and methanol. Methanol was added in amounts necessary to achieve the desired concentrations. Then, ~20 g of the dried close-packed PMMA colloidal crystals were soaked in this clear solution for 1−2 min. Excess solution was removed from the impregnated colloidal crystals by vacuum filtration. The composite sample was allowed to dry in air at room temperature for 24 h. Calcination was then carried out in a tube furnace with an air flow of ~12 mL min^{-1}. In a typical calcination, the temperature was increased from ambient at a rate of 2 °C min^{-1}, held at 325 °C for 3 h, increased at a rate of 2 °C min^{-1}, held at the desired final temperature for 2 h, and then allowed to cool to ambient temperature at a rate of 10 °C min^{-1}. The product samples designations are of the form MZr*x*HS*y*_*T*, where M stands for macroporous; *x* and *y* are the concentrations of Zr^{4+} and the sulfate ion in the precursor solution, respectively; and *T* is the final calcination temperature used. For example, the macroporous sample MZr1.25HS2.50_600 was produced by calcination at 600 °C of an amorphous composite prepared by using a 30 mL of precursor solution containing 1.25 M Zr^{4+}, 2.50 M H_2SO_4, methanol, and PMMA latex.

Characterization Methods. Scanning electron micrographs were obtained using a Hitachi S-800 field emission SEM operating at 15 kV. Samples for SEM were dusted on an adhesive conductive carbon disk attached to an aluminum mount. The samples were then coated with 10 nm of Pt. Transmission electron microscope (TEM) images were recorded using a slow-scan CCD on a Philips CM30 TEM operating at 300 kV with a LaB_6 filament. Samples for TEM imaging were prepared by sonicating about 20 mg of the powder in 20 mL of absolute ethanol for 1 min and then depositing a drop of the suspension on a holey carbon grid. Thermogravimetric analysis (TGA) and differential scanning calorimetry (DSC) were performed on a Netzsch-STA 409 PC simultaneous TGA/DSC thermal analyzer. The samples were heated under air flow from 30 to 800 °C at 10 °C min^{-1} in alumina crucibles. Nitrogen adsorption measurements were performed on an RXM-100 sorption system (Advanced Scientific Designs, Inc.) or a Micromeritics ASAP 2000 V3.00 sorption analyzer utilizing Brunauer−Emmett−Teller (BET) calculations for surface areas. Chemical elemental analyses for carbon and sulfur were carried out by Atlantic Microlabs Inc., Norcross, GA. Powder XRD measurements were performed on a Siemens D5005 wide-angle XRD spectrometer with Cu Kα radiation. Average particle size determinations were based on fitting the XRD patterns as Voigt functions with a quadratic background using the JADE program. The volume fractions of the monoclinic phase of zirconia within the crystalline walls were determined using the following equation[18,19]

$$v_m = \frac{1.311X_m}{1 + 0.311X_m} \quad (1)$$

where the intensity ratio X_m is defined as

$$X_m = \frac{I_m(\bar{1}11) + I_m(111)}{I_m(\bar{1}11) + I_m(111) + I_t(111)} \quad (2)$$

and I_m and I_t are the integrated peak intensities of the major monoclinic and tetragonal reflections, respectively.

n-Butane isomerization was carried out in a U-shaped stainless steal microreactor (8 mm i.d.) operated at atmospheric pressure. The catalyst (typically 0.6 g) was placed in the reactor between quartz wool plugs and activated for 4 h in flowing oxygen (35 mL min^{-1}) at 400 °C. The samples were subsequently cooled to the reaction temperature of 180 °C under continued oxygen flow. The reactor was purged with helium for 30 min before the introduction of the reaction

(11) Hino, M.; Arata, K. *J. Chem. Soc., Chem. Commun.* **1980**, 851−852.
(12) Livage, J.; Henry, M.; Sanchez, C. *Prog. Solid State Chem.* **1988**, *18*, 259−341.
(13) Yoldas, B. E. *J. Mater. Sci.* **1986**, *21*, 1080−1086.
(14) Ward, D. A.; Ko, E. I. *J. Catal.* **1994**, *150*, 18−33.
(15) Blanford, C. F.; Schroden, R. C.; Al-Daous, M. A.; Stein, A. *Adv. Mater.* **2001**, *13*, 26−29.
(16) Schroden, R. C.; Al-Daous, M. A.; Blanford, C. F.; Stein, A. *Chem. Mater.* **2002**, *14*, 3305−3315.
(17) Zou, D.; Ma, S.; Guan, R.; Park, M.; Sun, L.; Aklonis, J. J.; Salovey, R. *J. Polym. Sci. A: Polym. Chem.* **1992**, *30*, 137−144.
(18) Ward, D. A.; Ko, E. I. *Chem. Mater.* **1993**, *5*, 956−969.
(19) Toraya, H.; Yoshimura, M.; Somiya, S. *J. Am. Ceram. Soc.* **1984**, *67*, C-119−C-121.

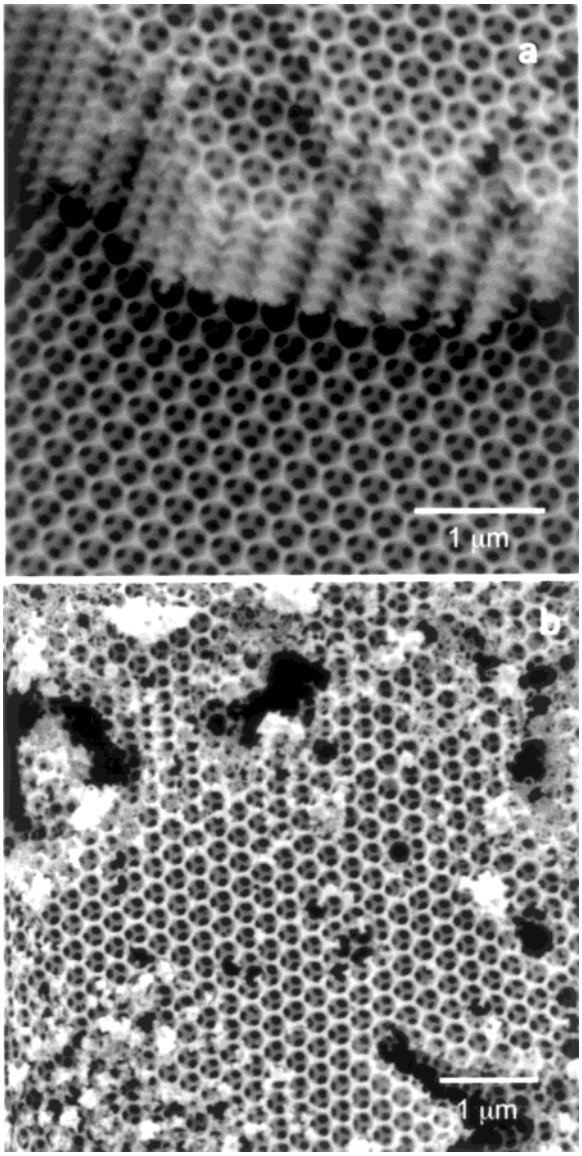

Figure 1. SEM images of (a) MZr1.25HS2.50_600 and (b) MZr1.25HS2.50_700.

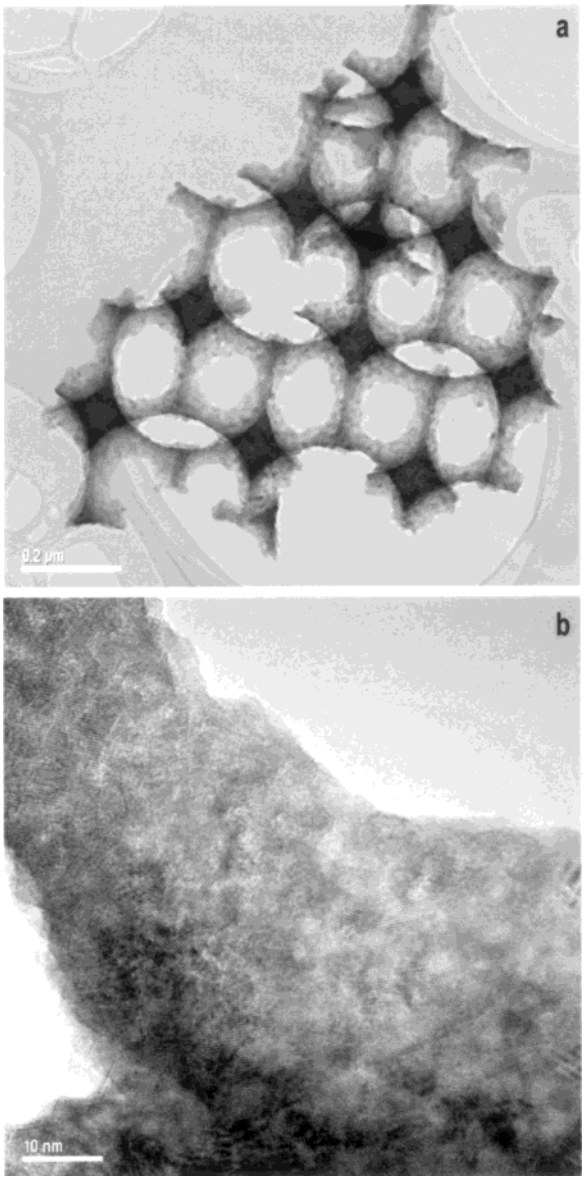

Figure 2. TEM images of MZr1.50HS3.00_600 showing (a) arrangement and structure of macropores and (b) wall structure composed of small agglomerated crystallites.

mixture of 1 mL min^{-1} of *n*-butane (Air Products & Chemical Inc., chemically pure) and 4 mL min^{-1} of He (Air Products & Chemical Inc.), corresponding to a WHSV of 0.25 g of butane per gram of catalyst per hour. It was verified that, under these reaction conditions, diffusional limitations were absent. The reaction products were analyzed with a gas chromatograph (Hewlett-Packard 5890A) equipped with a TC detector, using a Supelco packed column to separate the products. Conversion and selectivity were calculated on the basis of carbon number.

Results and Analysis

Macro- and Microstructure. The macroscopic structure of the product material is predetermined by the arrangement of the latex sphere template. This structure, depicted by the SEM micrographs in Figure 1 and the TEM image in Figure 2a, is composed of several layers of close-packed air voids ~300 nm in diameter surrounded by smooth, spherical walls and interconnected through windows to form the 3DOM structure. Depending on the calcination temperature of the material and the amount of sulfate added, structural shrinkage produced void diameters that were typically 7−35% smaller than the size of the latex spheres used. Table 1 lists shrinkage data that are averaged values measured by comparing a large number of pore center-to-center distances in the template-free samples with center-to-center distances in an array of templating latex spheres. Pore shrinkage was found to increase, for example, in the MZr1.25HS2.50 samples, from about 7% to about 21% with increasing calcination temperature from 450 to 650 °C. Meanwhile, for samples of the MZr1.25HS series calcined at 600 °C, the pore shrinkage was found to decrease from about 31% to about 13% as the SO_4/Zr molar ratio in the precursor solution increased from 0 to 3. In general, the extent of shrinkage decreased with increasing sulfate content and increased with increasing calcination temperature. In addition, for all samples, calcination temperatures of 700 °C or greater led to an extensive reduction in the fraction of ordered domains and the generation of debris on the external surface of the material, as shown in Figure 1b. Another factor found to affect the shrinkage and order of the macropores was the concentration of zirconium in the precursor solution used, where higher concentrations produced

Table 1. Summary of the Synthesis Conditions and Physicochemical Properties

sample	macropore shrinkage (%)	average crystallite size (nm)[a]	monoclinic volume fraction (%)	sulfur (wt %)	carbon (wt %)	BET surface area (m^2/g)	apparent SO_4 surface density (nm^{-2})
MZr1.25HS000_600	30.66	ND	28.5	0	<0.1	30.2	NA[b]
MZr1.25HS000_650	32.95	ND	33.7	0	<0.1	20.8	NA
MZr1.25HS000_700	34.86	ND	45.5	0	<0.1	5.3	NA
MZr1.25HS1.25_550	16.3	7.0	0	7.87	0.20	54.2	27.3
MZr1.25HS1.25_600	22.73	ND	7.7	1.50	0.14	97.3	2.90
MZr1.25HS1.25_650	30.33	ND	11.1	1.30	<0.1	118	2.07
MZr1.25HS2.50_450	7.20	small	0	12.15	0.25	37.70	60.63
MZr1.25HS2.50_550	10.91	6.3	0	10.14	0.19	43.3	44.06
MZr1.25HS2.50_600	16.84	7.2	0	3.48	0.11	98.6	7.02
MZr1.25HS2.50_650	20.61	ND	5.2	2.05	<0.1	123	3.10
MZr1.25HS2.50_700	30.05	ND	12.7	0.63	<0.1	70.90	1.67
MZr1.25HS3.75_550	10.50	small	0	12.05	0.15	37.5	60.45
MZr1.25HS3.75_600	12.64	6.7	0	4.92	0.10	79.2	10.86
MZr1.25HS3.75_650	18.20	7.8	0	2.43	<0.1	119	3.84
MZr1.50HS3.00_600	10.97	6.9	0	2.96	0.12	94.5	5.89
Zr1.25HS2.50_550	NA	6.9	0	9.72	ND[c]	7.84	ND
Zr1.25HS2.50_600	NA	7.4	0	3.55	ND	13.7	ND
Zr1.25HS2.50_650	NA	ND	7.1	2.32	ND	20.4	ND

[a] This value refers to the crystallite size in material with 100% tetragonal phase only. When mixed phases were present crystallite sizes were not calculated. [b] NA = not applicable. [c] ND = not determined.

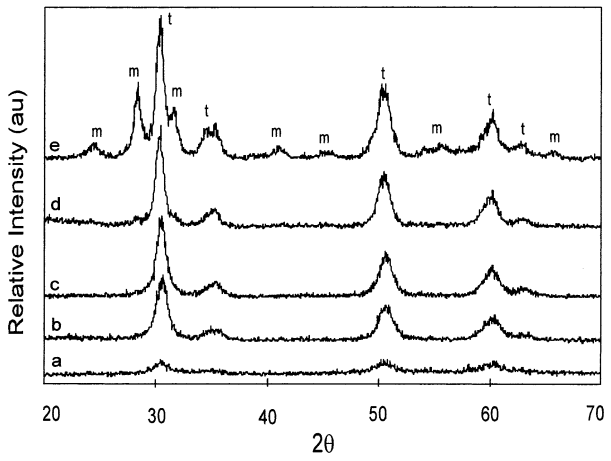

Figure 3. Powder XRD patterns of 3DOM sulfated zirconia prepared by calcination in air for 2 h at (a) 450, (b) 550, (c) 600, (d) 650, and (e) 700 °C (the MZr1.25HS2.50 series). Reflections from the tetragonal phase are marked with t and those from the monoclinic are marked with m.

materials with greater order and relatively less shrinkage (compare MZr1.50HS3.00_600 and MZr1.25HS2.50_600).

The wall structure of the macroporous solid is polycrystalline, with crystals smaller than the average wall thickness, as shown in the TEM images in Figure 2a and b. The average size of these crystals, measured by XRD line broadening and listed in Table 1, increased with calcination temperature and decreased with higher sulfate content. Typical XRD patterns, depicted in Figure 3 for the MZr1.25HS2.50 samples, show the initial crystallization of the amorphous precipitate into the tetragonal phase (PDF#42-1164), followed by gradual grain growth with increasing calcination temperature. Starting at ca. 600−650 °C, the tetragonal phase transformed partially to the more thermodynamically stable monoclinic crystalline phase (PDF#37-1484) accompanied by additional grain growth. The extent of grain growth and the volume fraction of the monoclinic phase present in the product were reduced with increasing sulfate content in the precursor solution. It is well-known that the presence of sulfate ions inhibits the initial amorphous-to-tetragonal crystallization and stabilizes the tetragonal crystalline phase by retarding the tetragonal-to-monoclinic transformation.[2,3,18,20] This was evident, for example, for the samples in the MZr1.25HS series calcined at 600 °C, which showed a decreasing average crystallite size with increasing sulfate content, along with a reduction in the extent of monoclinic phase formation or complete elimination of that phase. Corresponding samples synthesized without a template crystallized in a manner similar to their templated counterparts.

Thermal Analysis. To shed light on the mechanism behind the formation of the templated 3DOM materials, thermochemical transformations were followed by combined TGA/DSC analysis. Figure 4a and b shows the TGA/DSC graphs obtained for MZr1.25HS0.00 and MZR1.25HS2.50, respectively. The first weight loss region in the TG curve, exhibited by all samples, occurred between 85 and 210 °C and is most likely due to desorption of molecular and crystalline water from the sample.[2,5] The second weight loss region, which accounted for ∼60−77% of the sample's total weight and occurred in the temperature range of 340−420 °C for MZr1.25HS2.50 and 270−405 °C for MZr1.25HS0.00, is associated with the oxidative decomposition of the PMMA template.[21] The corresponding differential thermal gravimetric (DTG) curves show a single peak with a minimum at 390 °C for MZr1.25HS2.50, relating to the highest rate of polymer loss, and two separate peaks for the sample with no sulfate added. At higher temperatures, the TG curve for MZr1.25HS2.50 exhibited two other regions of weight loss; the first began at about 420 °C, had a maximum around 479 °C, and accounted for ∼4−5% of the weight loss. This weight loss and the temperature corresponding to its minimum in the DTG curve increased with sulfate content in the precursor solution. The last weight loss region occurred between 688 and 740 °C and accounted for another 4−5.5% weight loss. On the basis of reported analyses, the

(20) Morterra, C.; Cerrato, G.; Pinna, F.; Signoretto, M. *J. Catal.* **1995**, *157*, 109−123.
(21) Yan, H.; Blanford, C. F.; Lytle, J. C.; Carter, B.; Smyrl, W. H.; Stein, A. *Chem. Mater.* **2001**, *13*, 4314−4321.

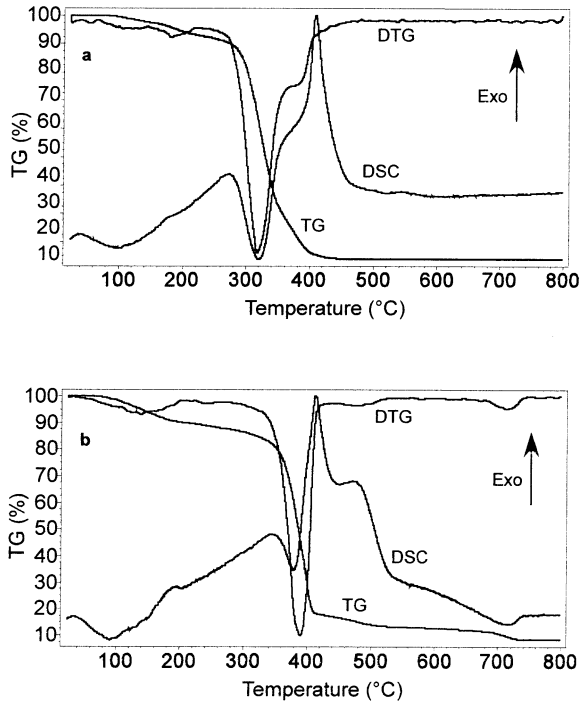

Figure 4. Thermal analysis data of (a) MZr1.25HS0.00 and (b) MZr1.25HS2.50, showing TGA, DSC, and DTG curves.

former region is assigned to sulfate migration from the bulk to the surface upon crystallization of the amorphous phase, a process that is accompanied by the elimination of sulfate ions; the latter weight loss is due to decomposition of the remaining sulfate groups from the sample.[18,22]

The corresponding DSC graphs started with an endothermic reaction centered at ~95 °C and an exothermic one at ~190 °C associated with the volatilization of physically adsorbed and crystalline water, respectively.[5] At higher temperatures, three major thermal reactions coinciding with polymer weight loss occurred for MZr1.25HS2.50 at 346 °C (exothermic), 378 °C (endothermic), and 413 °C (exothermic) and for MZr1.25HS000 at 275 °C (exothermic), 319 °C (endothermic), and 368 °C (exothermic). The lower-temperature exothermic reaction is due to the combustion of PMMA in air.[21] However, when the decomposition products displaced the limited amount of air present, the PMMA started to decompose through depolymerization in an endothermic step.[21] Eventually, more air reached the sample, and the higher-temperature exotherm corresponded to air combustion of the remaining carbonaceous deposits embedded in and stabilized by the inorganic matrix. These particular thermal events were not detected in sulfated samples synthesized without a latex template. Figure 4a and b indicates the presence of an additional exothermic event occurring at 407 and ~475 °C, respectively. This reaction did not coincide with a weight loss region in the TGA for the sample without sulfate and overlapped with the 4−5 wt % loss in the sulfated samples, as mentioned above. Moreover, the occurrence of this event shifted to the higher temperature of ~487 °C for $SO_4/Zr = 3$. This reaction is generally attributed to the crystallization of

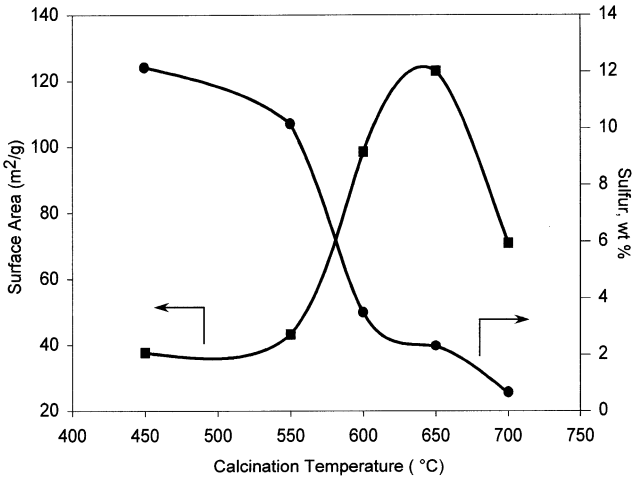

Figure 5. Amount of sulfate present and specific surface area formed as functions of calcination temperature for the MZr1.25HS2.50 series.

amorphous zirconia into the tetragonal phase,[2,5] which is delayed by the addition of the sulfate oxoanions and, as noted earlier, is accompanied by the elimination of the oxoanions.[5,22] On further heating, the last reaction resulted in a pronounced endothermic peak and corresponded to the thermal decomposition and loss of the remaining sulfate ions in the sample.[18,22] This endothermic reaction had a minimum that occurred typically at ~720 °C and, of course, was not present for the MZr1.25HS000 sample.

Elemental Analysis and Textural Properties. A typical crystalline product yield was about 10 wt % of the starting amorphous, latex-containing composite. Elemental analysis results for sulfur and residual carbon in the product materials are listed in Table 1. For each calcination temperature, the sulfur content correlated to the amount of sulfate in the initial precursor solution, i.e., it was larger in samples made of precursor solutions with higher SO_4/Zr molar ratios. The sulfur content decreased with increasing calcination temperature of the material.

The textural properties of the wall structure were investigated by nitrogen adsorption measurements where a type-II isotherm was typically observed. Table 1 lists the BET surface areas of samples prepared under various synthesis conditions. Surface areas as high as 123 m^2/g were obtained. Conventional syntheses produce materials with comparable or higher surface areas by careful precipitation of the precursor,[5] by using supercritical drying to form an aerogel,[18] or by thermal decomposition of zirconium sulfate salts at temperatures greater than 730 °C.[23,24] However, none of these techniques is readily amenable to colloidal crystal templating.

The effect of calcination temperatures on surface area and residual sulfur content is illustrated in Figure 5. The surface area increased with calcination temperature for the latex-templated sulfated samples and then decreased at a calcination temperature of 700 °C. It must be noted that the initial increase in surface area with temperature could not be attributed to remnant

(22) Afanasiev, P.; C., G.; Breysse, M. *J. Mater. Chem.* **1994**, *4*, 1653−1657.

(23) Fraenkel, D. *Ind. Eng. Chem. Res.* **1997**, *36*, 52−59.

(24) Arata, K.; Hino, M.; Yamagata, N. *Bull. Chem. Soc. Jpn.* **1990**, *63*, 244.

amorphous carbon, because the carbon content of the samples was less than 0.2 wt % after calcination at 550 °C and decreased at higher temperatures. However, by correlating the resulting surface area with the amount of sulfate in the sample, it is clearly seen that, as long as most of the sulfate was present, the surface area remained low and nearly constant but started to rise when the majority of the sulfate was lost, passing through a maximum when only a few percent of the sulfate remained. Then, the surface area started to decrease with further loss of residual sulfate.

Such a "bell-shaped" behavior of surface area as a function of temperature has been observed for sulfated metal oxides prepared by thermal decomposition of the corresponding metal-sulfate salts.[23] Although our initial precipitate was not crystalline but amorphous matter that crystallized into the tetragonal phase, its thermochemical behavior was analogous to that of the reported crystalline zirconium sulfate salt.[23] As reported, the surface area values on the lower-temperature portion of the bell-shaped curve correspond to the combined surface area of two phases, zirconium oxide containing buried sulfate and sulfated zirconia. The high-temperature portion of the surface area curve reflects lattice sintering, which is interrelated with the low sulfur content, the appearance of the monoclinic crystalline phase, and the formation of large grains.

This behavior was also observed for samples synthesized without the PMMA template, Zr1.25HS2.50, which have surface area values almost an order of magnitude smaller than those of their templated counterparts. On the other hand, samples synthesized with a PMMA template but without added sulfates (MZr1.25HS0.00) were found to have relatively low surface areas that decreased with calcination temperature; this behavior is expected on account of the absence of sulfate groups necessary to retard sintering.[2,5]

Catalytic Activity. Sulfated zirconia is one of the most active materials for catalyzing *n*-butane isomerization. This characteristic reaction was, therefore, chosen to evaluate the catalytic activity of the material. The catalysts' performance was examined as a function of both calcination temperature and initial SO_4/Zr molar ratio used in the precursor solution. Figure 6a depicts the reaction results, in terms of the rate of *n*-butane converted to isobutane. The conversion profiles show strong catalyst decay during the first 50 min on stream, followed by a slower deactivating region. The initial high rates of conversion can be interpreted in terms of the low initial isobutane selectivity shown in Figure 6b, where propane, pentane, and methane were obtained as the minor products. Isobutane selectivity increased with time on stream and reached ~92% by samples calcined at 600 °C. All of the samples maintained their 3DOM structure after the catalytic reactions.

By concentrating on the relatively flatter sections of the conversion plots in Figure 6a, the rate of *n*-butane conversion to isobutane at ~100 min provides a useful means of comparing the catalytic activities of the various materials as a function of calcination temperature.[20] Figure 7 shows that the rate of conversion initially increased with calcination temperature for the series of MZr1.25HS2.50 samples. The conversion rate reached a maximum for the sample calcined at 600 °C

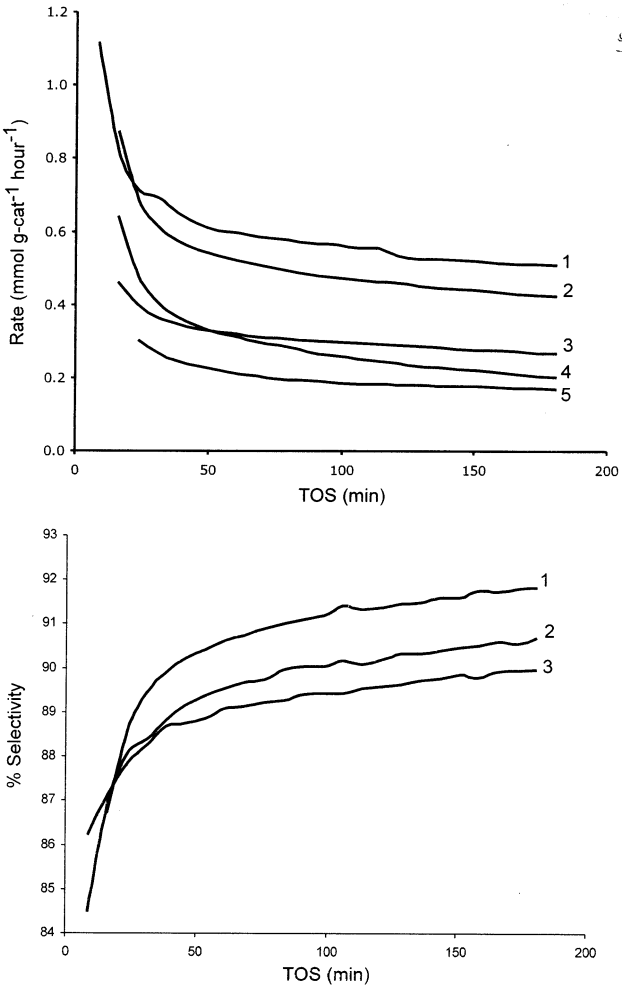

Figure 6. (a) Rate of *n*-butane isomerization as a function of time on stream for (1) MZr1.25HS2.50_600, (2) MZr1.25HS2.50_550, (3) MZr1.25HS2.50_650, (4) MZr1.25HS3.75_600, and (5) MZr1.25HS1.25_600. (b) Isobutane selectivity for (1) MZr1.25HS2.50_600, (2) MZr1.25HS2.50_550, and (3) MZr1.25HS2.50_650.

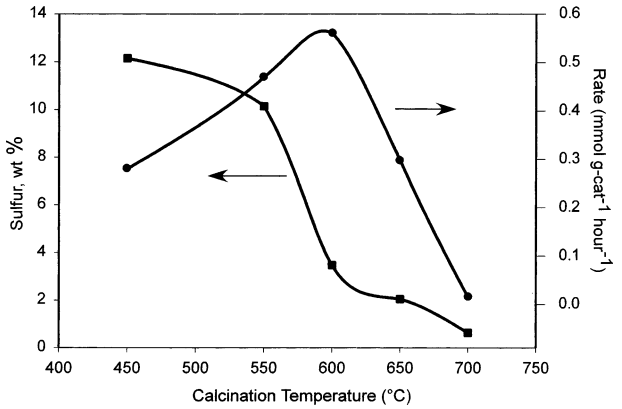

Figure 7. Effect of calcination temperature on the rate of *n*-butane isomerization and the amount of sulfate present for the sample series MZr1.25HS2.50. Conversion data were taken at 100 min on stream.

and then decreased at higher calcination temperatures; samples calcined at 700 °C were found to be inactive. Similar trends were also observed for the other sets of samples prepared with different SO_4/Zr ratios. It should be noted that the maximum activity did not coincide with the maximum surface area, because calcination

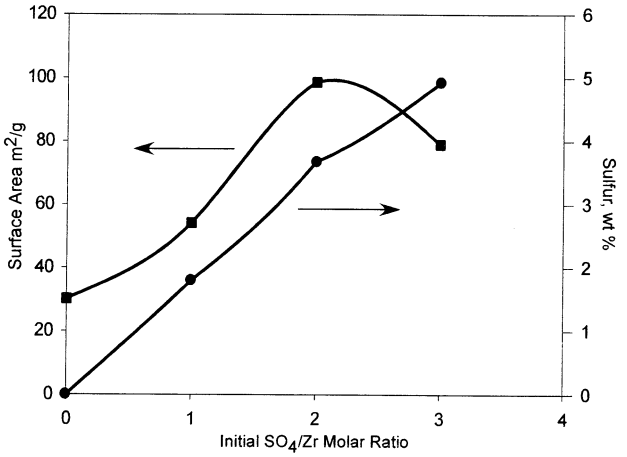

Figure 8. Amount of sulfate present and specific surface area formed as functions of initial SO_4/Zr molar ratio in the precursor solution for samples calcined at 600 °C.

temperatures of 650 °C and higher caused greater loss of sulfate species, leading to increased volume fractions of the catalytically less active monoclinic phase.

The effect of varying SO_4/Zr ratios on *n*-butane conversion can also be deduced from the data in Figure 6a. For the MZR1.25HS series calcined at 600 °C, *n*-butane conversion increased in the order of $SO_4/Zr = 1 < 3 < 2$. This result can be rationalized by considering the surface area and the amount of sulfate present as functions of the initial SO_4/Zr molar ratio, as shown in Figure 8. Once again, the surface area follows a bell-shaped curve with a maximum for the sample with $SO_4/Zr = 2$. The amount of sulfate present, however, increases monotonically with the initial SO_4/Zr ratio. For the case of $SO_4/Zr = 1$, the low reaction activity can be attributed to the small amount of sulfate present, which apparently was not sufficient to impede grain growth and, hence, led to the formation of about 11 vol % monoclinic phase and a reduction in the surface area of the material. For the case of $SO_4/Zr = 3$, thermal development was delayed compared to samples with lower initial sulfur content. Thus, at 600 °C, the sulfate content of this sample was still relatively high, suggesting that some sulfate must be present in the bulk, limiting crystallization and catalytic activity.

Discussion

Using the concept of sulfate surface concentration, a value of 3.2−4 nm^{-2} has been considered to represent monolayer coverage by isolated sulfate species.[25] The calculated apparent surface sulfate densities for our samples are listed in Table 1. These values are based on the total amounts of sulfur in the samples and can therefore also include contributions from bulk sulfate, in particular for samples calcined at the lower temperatures. Samples with surface sulfate concentrations of 3.2 nm^{-2} or less contained a certain volume fraction of the monoclinic phase. This phase was absent in samples with larger sulfur concentrations, which exhibited progressively smaller crystallite sizes as the concentration increased. This variation in crystallite size affected the extent of macropore shrinkage. Apparently, an increase in wall crystallite size led to a reduction in the average macropore diameters, associated with increased wall densities. In particular, relatively high calcination temperatures produced excessive crystallite growth as a result of sulfate decomposition and crystallite coalescence, which led to the appearance of the monoclinic crystalline phase, the collapse of some macropores, the generation of debris, and the deterioration of the long-range order of the macroporous material.

The inhibiting effect of sulfate groups on crystal growth, and therefore on the effective surface area, is not sufficient to explain the relatively low surface area values obtained for the sulfated samples made without a PMMA template (Zr1.25HS2.50). We believe that the inherent porosity of the PMMA template also contributed to the surface area formation. Samples prepared with methanol in the precursor mixtures exhibited higher surface areas and greater product yields than samples made without methanol. Methanol acts as a wetting and swelling agent and is believed to enhance the penetration of the inorganic precursor solution into the latex spheres, forming an outer organic−inorganic composite rim. Upon calcination, this outer rim turns into the inner porous walls of the 3DOM structure, as shown in Figure 2a.

In support of this argument, TGA/DSC results showed that, in the sample made with PMMA and no sulfate, the crystallization temperature was not sufficiently separated from the temperature of the polymer decomposition process. Hence, as the polymer was thermally removed, the crystals started to grow unhindered to fill the space left behind. In contrast, the temperature separation between the two thermal processes was greater for the sulfated PMMA-templated samples, and the sulfates accumulating on the surface of the formed crystallites acted as barriers preventing the coalescence of these crystallites and preserving the pores generated by the thermal decomposition of the embedded PMMA.

One further point concerns the relationship between the catalytic activity and the sulfate concentration. It was found that an apparent sulfate density greater than ∼4 nm^{-2} and less than ∼11 nm^{-2} produced the most catalytically active materials. In particular, MZr1.25HS2.5_600 with a sulfate density of ∼7 nm^{-2} seemed to be the most active of all the samples. Samples with sulfate densities of less than ∼3.2−4 nm^{-1} contained significant amounts of the monoclinic phase and therefore exhibited lower catalytic activity.[14] Sulfate densities greater than ∼11 nm^{-2} are indicative of bulk sulfate and poorly developed, low-surface-area materials, which also exhibited low catalytic activity.[25,26]

Conclusion

We have described a colloidal crystal-templating synthesis that produced three-dimensionally ordered macroporous, crystalline, and catalytically active sulfated zirconia. Series of samples with different sulfate ion concentrations were synthesized and applied as catalysts in the gas-phase isomerization of *n*-butane. The calcination temperature was found to have a strong effect on the amount of the sulfate ions present in the

(25) Katada, N.; Endo, J.-i.; Notsu, K.-i.; Yasunobu, N.; Naito, N.; Niwa, M. *J. Phys. Chem. B* **2000**, *104*, 10321−10328.

(26) Farcasiu, D.; Qi Li, J.; Cameron, S. *Appl. Catal. A* **1997**, *154*, 173−184.

final crystalline product. This, in turn, influenced the various physicochemical properties of the resulting materials. The amount of sulfate present decreased with calcination temperature, and the sulfate density was sensitive to the SO_4/Zr molar ratio in the precursor solution. The sulfate species limited the size of the resulting crystallites, which, in turn, led to less macropore shrinkage and produced structures with greater periodic order.

The combined effects of the added sulfate and the latex-induced porosity are believed to be the main causes for the generated surface area of the material. Typical surface area values for the templated materials were comparable with those of other active sulfated zirconia materials, but were significantly larger than those of their nontemplated counterparts. They exhibited a bell-shaped behavior as a function of calcination temperature, where both the starting amorphous precipitate and the final zirconium oxide product had low surface areas. The higher surface areas, peaking at 118−123 m^2/g, were associated with sulfated zirconium oxides produced at a calcination temperature of 650 °C and a sulfate density of ∼2−4 nm^{-2}. The catalytic activity also exhibited a bell-shaped behavior as a function of sulfate density and calcination temperature, where maximum reaction rates were found to occur for samples calcined at 600 °C with a sulfate density of ∼ 7 nm^{-2}.

Acknowledgment. We thank the U.S. Army Research Laboratory and the U.S. Army Office under Contract/Grant DAAD 19-01-1-0512, the National Science Foundation (DMR-9701507), the MRSEC Program of the NSF (DMR-9809364), and the David and Lucile Packard Foundation for support of this research. C. F. Blanford is acknowledged for obtaining the TEM images.

CM030019B